Nanomaterials and Nanotechnology

OPEN ACCESS
ARTICLE

Polyol-based Synthesis of Praseodymium Oxide Nanoparticles

Invited Article

Caroline Quievryn[1], Samuel Bernard[1,*] and Philippe Miele[1]

1 IEM (Institut Europeen des Membranes), UMR 5635 (CNRS-ENSCM-UM2), Universite Montpellier 2, Montpellier, France
* Corresponding author E-mail: Samuel.bernard@univ-montp2.fr

Received 15 Nov 2013; Accepted 7 Mar 2014

DOI: 10.5772/58458

Abstract A series of well-crystallized praseodymium oxide (Pr_6O_{11}) nanoparticles are synthesized via a highly scalable process from praseodymium nitrate. Praseodymium hydroxide is synthesized through a modified polyol process and subsequent calcination in air at 600°C for 2 h to transform the precursor material into Pr_6O_{11} nanoparticles. A complete characterization of a specific sample by SEM, HRTEM, and X-ray diffraction (XRD) demonstrates that Pr_6O_{11} nanoparticles form elementary blocks with a calculated size of 118 nm, containing slightly agglomerated nanocrystalline particles with a polycrystalline face-centred cubic phase and an individual size of around 10 nm. Particles can be easily dispersed in water through ultrasonification. Particles display a BET Specific Surface Area (SSA; 8.75 $m^2\ g^{-1}$) with a nitrogen adsorption-desorption isotherm of type II and a helium density of powders (d = 5.66 g cm^{-3}).

Keywords Polyol, Praseodymium Nitrate, Praseodymium Oxide, Nanoparticles, Calcination

1. Introduction

Over the past few years, praseodymium oxide (Pr_6O_{11}) has been applied in different application domains such as sensors [1], high-temperature pigments [2], catalysts [3,4] and oxygen storage components of three-way automotive catalysts [5]. For such applications, nanosized materials are attractive because of the possibility to tune their physico-chemical properties in terms of shape, size and surface-to-volume ratio.

Pr_6O_{11} is conventionally prepared by solid-state reactions [6-8], a molten salt method [9], template-free precipitation [10], or sol-gel coupled with a shaping process such as electro-spinning [11]. A relatively recent paper has illustrated the possibility of preparing nanostructured Pr_6O_{11} via two traditional methods (calcination of the nitrate and a sol-gel method) and two more sophisticated, modern techniques (citric method and polymerized precursor route/modified Pechini method) [12]. The praseodymium precursor used as a starting material for the synthesis in all cases was praseodymium nitrate $Pr(NO_3)_3.6H_2O$. As far as we know, there is a very limited number of methods that have been reported in the literature for the synthesis of Pr_6O_{11} nanopowders, although such nanomaterials are expected to provide access to a wider range of applications in set-up devices such as sensors or dispersed in porous ceramic supports to act as a catalyst. A major reason for this is that a reliable shape-, size- and phase-controlled synthesis

process leading to the synthesis of nanosized Pr_6O_{11} powders is still not available. Usually, direct heat-treatment of praseodymium nitrate hexahydrate $Pr(NO_3)_3{\cdot}6H_2O$ leads to micron-sized Pr_6O_{11} powders. In addition, both direct precipitation of $Pr(NO_3)_3{\cdot}6H_2O$ into praseodymium hydroxide $Pr(OH)_3$ nanoparticles and synthesis of $Pr(OH)_3$ nanoparticles in reverse micelles followed by heat-treatments lead to loss of nanoparticle cohesion, i.e., formation of nanorods. Within this context, developing a new and simple method for synthesis of Pr_6O_{11} particles on the nanoscale could thus open up new avenues for uncovering their remarkable properties and for achieving useful applications.

Inorganic nanomaterials can, in principle, be synthesized using both top-down and bottom-up techniques. The bottom-up strategy uses the techniques of molecular synthesis [13], colloid chemistry [14], polymer science [15], and related areas to make structures with nanometre dimensions. The top-down strategy [16] uses miniaturizing techniques such as machining, templating or lithography to pattern materials. Self-assembly [17-19] bridges these two techniques and allows materials to be designed with hierarchical order and complexity. The use of organic surfactants and polymers in self-assembled nanoparticle synthesis has been a popular method of achieving morphological control, where the polymer or foreign ions typically work to regulate and stabilize the surface of nanoparticles. One of the most common and easy approaches that utilize this strategy is the polyol method [20].

Polyol synthesis is a chemical method involving forced hydrolysis of transition metal salts, which allows metal or metal oxide nanoparticles to be prepared with controlled size, texture and shaping [21-26]. Initial work on elemental metals or alloys exploited the reducing properties of a high-boiling alcohol (glycerol, glycol) towards a suitable metal precursor. Owing to their high dielectric constants, the alcohol acted as a solvent able to dissolve inorganic compounds, a growth medium and a complexing agent in some cases. Furthermore, owing to relatively high boiling points, such alcohol offered a wide operating-temperature range (from 25°C to the boiling point) for preparing inorganic compounds. It also often acted as a stabilizing agent that effectively limited particle growth and hindered inter-particle aggregation.

The polyol method holds promise as a low-cost, high-yield technique with a wide range of scientific and technological applications, which is ideal for potential industrial scale-up [27,28]. In the case of oxide synthesis, the polyol method can be considered as a sol-gel process carried out at relatively elevated temperature with accurate control of particle growth. It has been studied and reported for the synthesis of a wide range of oxide sub-micrometre particles, including Y_2O_3, ZnO, Mn_3O_4, $CoTiO_3$, V_xO_y, TiO_2, PbO and SnO_2 [29-36].

Ethylene glycol is among the most widely used solvents for the polyol synthesis of metal oxide nanoparticles due to its strong reducing capability, relatively high boiling point and high dielectric constant, which increases the solubility of inorganic salts [37]. Ethylene glycol is commonly used as a crosslinking reagent because of its propensity to coordinate with the central metal ion and form a metal glycolate leading to subsequent oligomerization [38]. It has also been demonstrated that as-synthesized glycolate precursors can later be converted to their more common metal oxide derivatives when calcined in air, while maintaining the original precursor morphology [35-39].

In this paper, we describe a fast, convenient and green synthetic route for the large-scale synthesis of praseodymium oxide nanoparticles with an individual size of approximately of 10 nm by polyol synthesis from praseodymium nitrate in diethylene glycol (DEG), and a subsequent addition of sodium hydroxide followed by calcination in air at 600°C. Thermogravimetric analysis and X-ray diffraction are combined to discuss the effect of both the nature of the Pr_6O_{11} precursor and the quantity of sodium hydroxide added to the praseodymium nitrate-DEG mixture; electron microscopy, EDS, and BET studies were used to characterize the structure, crystallinity, morphology, chemical composition and texture of the Pr_6O_{11} nanoparticles. Also, we note that our method provides nanoparticles that are stable and easily dispersed in water, and could be adapted to the preparation of coatings or porous materials.

2. Experimental procedure

All chemicals were purchase from Sigma Aldrich and used as received. The polyol method involves the reduction of a metal salt precursor by a polyol, a compound containing multiple hydroxyl groups. The polyol used in this synthesis, diethylene glycol ($(HOCH_2CH_2)_2O$-DEG, 99%), served as both reducing agent and solvent. 2.5 g of praseodymium nitrate (5.75 mmol, $Pr(NO_3)_3.xH_2O$, 99 %) was stirred in 50 mL of diethylene glycol for 30 min in a Schlenk flask (in air). The as-prepared solution was then treated at 140°C (in air). Sodium hydroxide (NaOH, with a controlled concentration in water) was added after a dwelling time of 1 h, and then the mixture was directly heated up to 180°C and kept at this temperature for 4 h, after which it was cooled naturally.

Pre- and post-calcined samples	Quantity of NaOH (mL)	[NaOH] (**mol/L**)
***A*-OH/*A*-Ox**	5	9
***A'*-OH/*A'*-Ox**	5	9
***B*-OH/*B*-Ox**	10	9
***C*-OH/*C*-Ox**	20	9
***D*-OH/*D*-Ox**	5	15
***E*-OH/*E*-Ox**	5	4

Table 1. Concentration and quantity of NaOH solution added during the synthesis

Following centrifugation, precipitation isolation, washing several times with ethanol, acetone then distilled water, and drying, as-obtained samples labelled ***X*-OH** (with X = A, B, C, D and E) were annealed at 600°C for 2 h in air (ThermoConcept, Germany) to form the corresponding oxide labelled ***X*-Ox**. Table 1 reports the quantities and concentrations of NaOH solution added during the synthesis of the different hydroxide and oxide samples. We compared the effect of the praseodymium oxide precursor on the (nano)structure and morphology of the final materials. Following the procedure described above, we investigated the synthesis of praseodymium oxide nanoparticles from praseodymium chloride ($PrCl_3$, 99 %) leading to the pre- (***A'*-OH**) and post-calcined (***A'*-Ox**) samples.

Thermogravimetric analysis (Hi-Res TGA 2950, TA Instruments,) of $Pr(OH)_3$ was performed with the sample ***E*-OH** under the following conditions: sample mass 14 mg, platinum crucible of 100 µl, heating rate 5°C min^{-1}, range 25-600°C, and an atmosphere of air (60 ml min^{-1}). The phase and crystallite size of the Pr_6O_{11} nanoparticles were studied using X-ray diffraction (XRD, PANalytical X'pert Pro MPD powder diffractometer with a detector X'celerator; CuKα radiation (λ_1 = 1.5406 Å, λ_2 =1.5444); the sample was scanned with CuKα radiation within the range of 10°-60° (2θ), with a step size of 0.017° and an exposure time of 50 s. The accelerating voltage and current were 40 kV and 30 mA, respectively. Phase identification was achieved by matching the patterns against stick patterns from the JCPDS database. A semi-quantitative estimation of the extent of crystallization in samples was achieved by calculating the integrated intensity of the (111) diffraction peak. The (111) diffraction peak was chosen for this purpose, based on two considerations: freedom from peak overlap and sufficient relative intensity. Special sample holders were used to irradiate a constant volume of sample powder to enable comparison of the integrated intensities of different samples. Crystallite sizes of Pr_6O_{11} were calculated from the FWHM of the above diffraction peak using the Scherrer formula. FWHM values were corrected for instrumental line broadening. The surface morphology of the nanoparticles was examined using scanning electron microscopy (SEM, Hitachi S4800) equipped with energy-dispersive spectroscopy analysis (EDS) to obtain information on the praseodymium and oxygen contents of the material. Transmission electron microscopy (TEM) was carried out on the sample ***E*-Ox** using a JEOL 1200 EXII operating at 200 kV. A solution of ethanol containing $Pr60_{11}$ particles was prepared via ultrasonic bath. Samples for TEM were prepared by spreading a drop of this solution on copper grids coated with a carbon film followed by evaporation under ambient conditions. The nitrogen adsorption/desorption isotherms of the sample ***E*-Ox** were measured on a Sorptomatic 1900 analyser (Fisons). Before adsorption measurements, all samples were out-gassed for 4 h at 150°C in the degas port of the adsorption analyser. The Brunauer–Emmett–Teller (BET) method was used to calculate the specific surface area.

3. Results and discussion

The reduction ability of reagents is critical in the control of the size and morphology of nanostructures. Herein, a modified polyol process was designed to synthesize Pr_6O_{11} nanoparticles. The Pr_6O_{11} precursor ($Pr(NO_3)_3$ or $PrCl_3$) was mixed with DEG ($(HOCH_2CH_2)_2O$) to be heated at 140°C before addition of controlled quantities and concentrations of NaOH and subsequent heating to 180°C. After a dwelling time of 4 h at 180°C, the mixture was cooled down to be calcined at 600°C in air.

Firstly, we have compared the effect of the nature of the Pr_6O_{11} precursor on the production of nanoparticles. In both cases, nanoparticles are obtained. However, whereas 2.5 g (5.75 mmol) of $Pr(NO_3)_3$ could be easily dissolved in 50 mL of DEG leading to samples ***A*-OH/*A*-Ox**, $PrCl_3$ was poorly soluble in DEG and only 0.5 g (1.34 mmol) of $PrCl_3$ could be dissolved in 50 mL of DEG). Within this context, the use of $PrCl_3$ to produce the samples ***A'*-Ox/*A'*-OH** is disadvantageous.

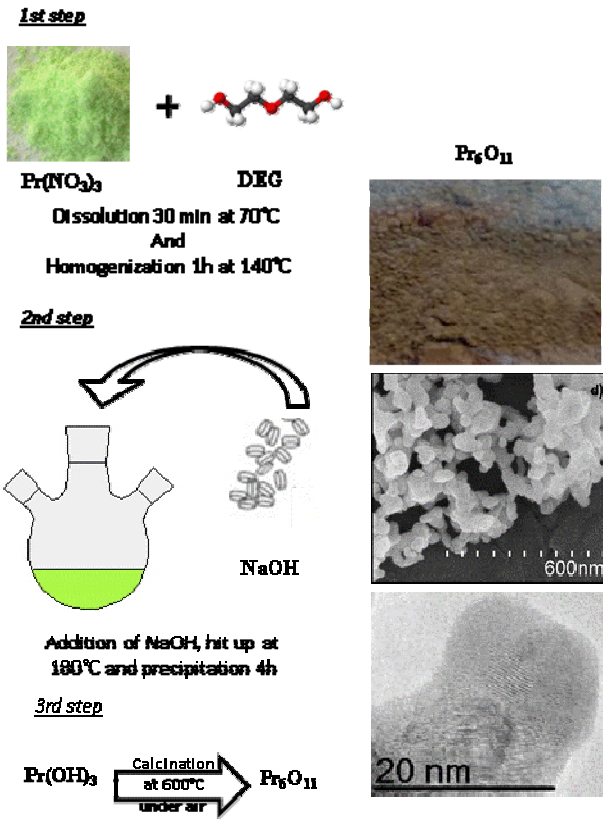

Figure 1. Overall synthetic path employed to generate Pr_6O_{11} nanoparticles

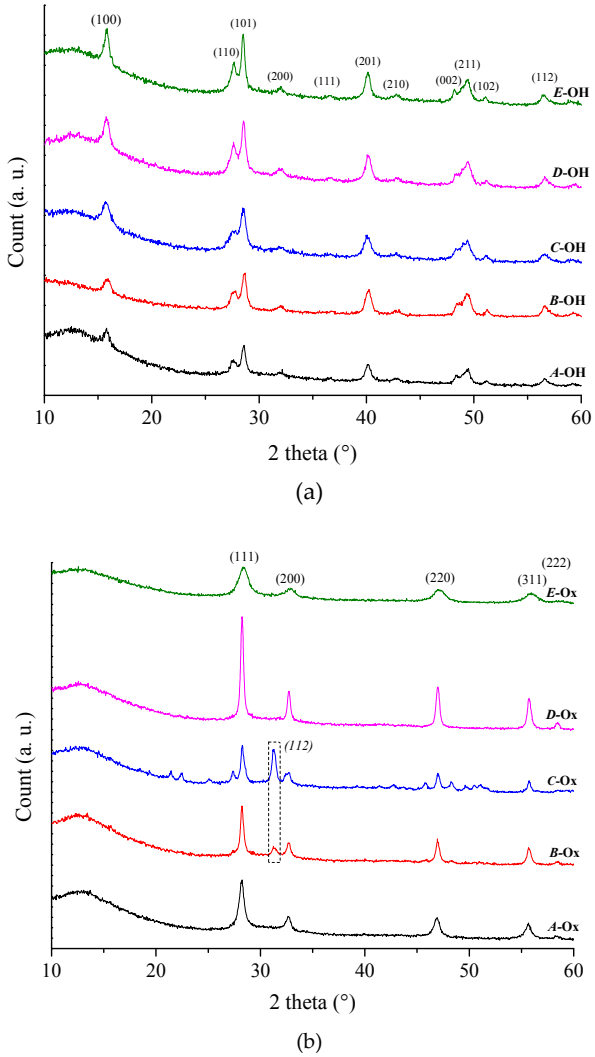

Figure 2. XRD patterns of the pre- (***X*-OH**, a) and post-calcined (***X*-Ox**, b) samples

The as-synthesized suspension from $Pr(NO_3)_3$ can be used as-is for coating-based processes such as spray-/dip- or spin-coating, or to infiltrate inorganic templates such as ordered mesoporous powders or materials with hierarchical porosity such as those we prepared in our group [40-46]. In the present paper, we obtained pre-calcinated powders by centrifugation, precipitation isolation, washing several times with ethanol, acetone and distilled water and drying, then additional heating to 600°C to obtain the required oxide nanoparticles (Figure 1).

In our process, the polarity of polyol offers the ability to dissolve praseodymium nitrate. As a high-boiling-point solvent, polyol provides a high-temperature environment and improves the reactivity of various reactants. In this work, DEG acted both as the solvent, as a reducing agent and as a growth medium. NaOH provided the hydroxyl ion to form $Pr(OH)_3$, as reported in Figure 2, which presents the XRD patterns of samples ***X*-OH**. Phase identification is achieved by locating the characteristic diffraction peaks of the respective phases in the XRD patterns. Prior to calcination, the phase was readily indexed for each sample to the hexagonal structure of praseodymium hydroxide consistent with the standard powder diffraction file of $Pr(OH)_3$ (JCPDS 83-2304) (Figure 2) with lattice parameters a = 0.6505 nm and c = 0.3428 nm, with no effect of the NaOH concentration and quantity on the peak numbers and positions.

During the subsequent calcination step, the removal of gaseous by-products induced a weight loss of 75% after thermal decomposition at 600°C (*see supporting information, Figure. 1SI*). The important weight loss is attributed to the presence of residual DEG trapped in the $Pr(OH)_3$ powders. This is clearly observed in the FTIR spectra of samples ***X*-OH** (*see supporting information, Figure. 2SI*). FTIR spectra exhibit the characteristic bands of $Pr(OH)_3$ at 1077 cm^{-1} (Pr-O bond stretching) and at 654 cm^{-1} (Pr-O bond deformation). Other bands are assigned to DEG, whereas the band at 3600 cm^{-1} can be attributed to DEG and $Pr(OH)_3$. After calcinations to 600°C, the obtained spectra are characteristic of Pr_6O_{11} with bands at 852 cm^{-1} (Pr-O bond deformation) and 1469 cm^{-1} (Pr-O bond stretching). The XRD patterns of the residues accurately reflected the IR spectra of samples ***X*-Ox**. This could be indexed to the pure face-centred cubic phase (space group: Fm3 m-225) with calculated lattice constant a = 0.54678 nm, which is consistent with the standard diffraction pattern of Pr_6O_{11} (JCPDS 42-1121) (Figure 2). There are no impurity phases of hydroxides and other oxides. The transition from the hydroxide precursor to crystalline Pr_6O_{11} was also noted, the sample changing colour from light green (pre-calcined) to dark brown (post-calcined). However, the XRD patterns of samples ***B*-Ox** and ***C*-Ox** showed a diffraction peak around 2θ = 31°. This peak can be assigned to sodium praseodymium oxide ($NaPrO_2$). EDX of the samples confirmed the presence of sodium. As reported in Table 1, these samples were prepared with the highest quantity of NaOH. This indicates that the quantity of NaOH needs to be controlled to obtain pure Pr_6O_{11}. Comparing the XRD patterns of samples ***A*-Ox**, ***D*-Ox**, and ***E*-Ox**, it is clear that the increased concentration of NaOH added during the synthesis caused sharpening of the diffraction peaks, the result of an increase in the crystallite sizes. Having concluded that both the quantity and concentration of NaOH has a strong effect on crystallization, it would be of significant importance to study the effect of these parameters on crystallite size on the samples ***A*-Ox**, ***D*-Ox**, and ***E*-Ox**. The crystallite size was determined by measuring the full width at half the maximum in conjunction with the Debye–Scherer formula. The values for crystallite size are reported in Table 2.

Name of the sample after calcination	Crystallite size (nm)
***A*-Ox**	14.3
***D*-Ox**	24.7
***E*-Ox**	7.2

Table 2. Calculated crystallite size in samples ***A*-Ox**, ***D*-Ox** and ***E*-Ox**

This clearly indicates the increase in crystallite size along with the concentration of NaOH used during the synthesis. There are no impurities detected by energy-dispersive X-ray spectroscopy (EDS) analysis (*see supporting information, Figure 3SI*) except for carbon elements arising from the carbon film in SEM observations.

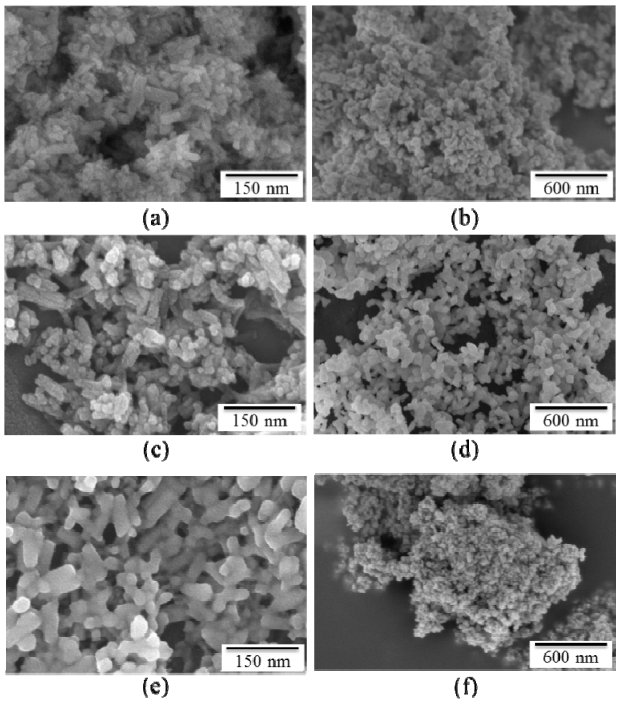

Figure 3. SEM micrographs of selected pre- and post-calcined samples ***A*-OH** (a), ***A*-Ox** (b) ***D*-OH** (c) ***D*-Ox** (d), ***E*-OH** (e) and ***E*-Ox** (f)

Figure 3 shows the scanning electron microscopy (SEM) images of the selected pre- and post-calcined samples ***A*-OH/*A*-Ox**, ***D*-OH/*D*-Ox** and ***E*-OH/*E*-Ox**. Pre-calcined nanostructures are mainly in the form of nanorods and are transformed by calcination at 600°C into nanoparticles. This means that the structure of $Pr(OH)_3$ collapsed during heat-treatment to 600°C, leading to the formation of spherical Pr_6O_{11} nanostructures, most probably due to the fact that it represented the most thermodynamically stable structure. The collected SEM micrographs of samples ***A*-Ox**, ***D*-Ox** and ***E*-Ox** showed that the particle population is relatively homogeneous, including small round-shaped particles and an extremely low proportion of particles of large size. The sample ***E*-Ox** displays the smallest individual particle sizes. The high-magnification SEM image of the sample ***E*-Ox** (Figure 4) shows that the sample was composed of nanoparticles aggregated in clusters. SEM is not really suited to observing nanosized materials, but it provides a view of the general particle population. Therefore, it is difficult to estimate the size of the individual particles.

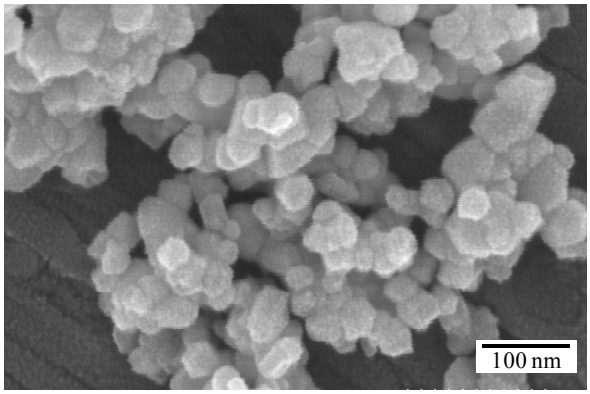

Figure 4. SEM micrographs of the sample ***E*-Ox**

We focused our study of the sample ***E*-Ox**. The TEM micrograph of the sample ***E*-Ox** was investigated to assess the morphology and the overall particle size of samples.

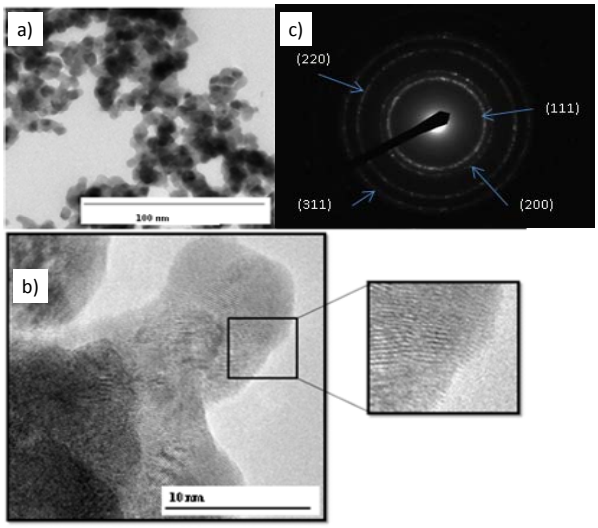

Figure 5. TEM micrographs of the sample ***E*-Ox** (a, b) with SAED pattern (c)

A typical bright-field TEM image of the sample ***E*-Ox** is shown in Figure 5. The micrograph shows that the obtained sample formed elementary blocks composed of a large amount of spherical-shaped nanoparticles with an average diameter of 9.4 ± 0.9 nm, as shown on the statistical histogram deduced from the TEM image (Figure 6). The corresponding selected area electron diffraction (SAED) pattern, inset in Figure 5, confirmed the identification of the face-centred cubic phase of Pr_6O_{11}. We investigated HRTEM to refine the structural information and to corroborate the SAED results. Figure 5

shows a high-resolution TEM (HRTEM) image used to gather information on powder nanostructure. The HRTEM image of the particle core demonstrates that the specimen consists of very fine nanocrystalline Pr_6O_{11}; the observed interplanar distance is d_{111} = 0.313 nm and the growth direction is along the <111>.

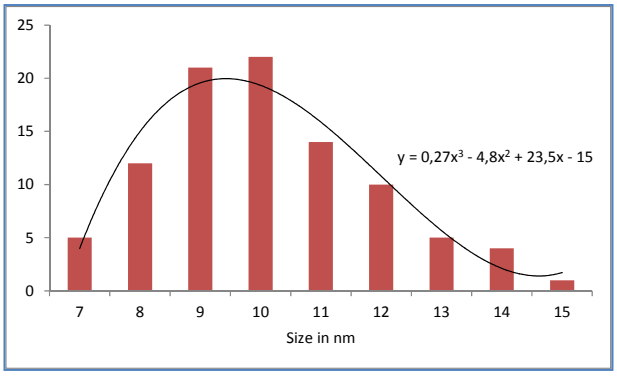

Figure 6. Histogram of the particle size deduced from TEM observations of the sample ***E*-Ox**

The sample ***E*-Ox** displayed a helium density of 5.66 g cm^{-3} and a BET specific surface area of 8.75 m^2 g^{-1}. A similar value is commonly found for nanosized powders [46-48]. Figure 7 shows the nitrogen adsorption-desorption isotherm, which is of type II according to the IUPAC classification [50,51], with an evident hysteresis loop in the 0.9 to 1.0 range.

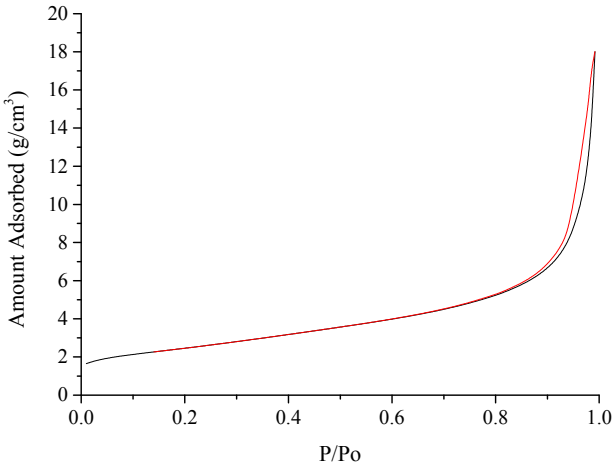

Figure 7. BET nitrogen adsorption-desorption isotherm curve for the Pr_6O_{11} nanoparticles

The form of the hysteresis loop suggests that the sample is basically non-porous and agglomerated. Assuming that the Pr6O11 nanoparticles are almost spherical, as confirmed by TEM, equation (1) shows how the SSA and density (d) can be used to calculate the Average Particle Size (APS in nm) of powders:

$$APS = 6000/(SSA*d)$$

An APS of 118 nm is calculated for Pr_6O_{11} nanoparticles.

4. Conclusions

In conclusion, this is a highly scalable and reproducible process for the synthesis of a series of high-purity and well-crystallized Pr_6O_{11} nanoparticles. We have described polyol synthesis from praseodymium nitrate in diethylene glycol (DEG) and the subsequent addition of sodium hydroxide, followed by calcination in air at 600°C to convert into praseodymium oxide (Pr_6O_{11}). The morphological and textural analyses of a specific sample showed that the sample formed elementary blocks with a calculated average aggregate size of 118 nm based on the BET Specific Surface Area (SSA; 8.75 m^2 g^{-1}) and the helium density of powders (d = 5.66 g cm^{-3}). These elementary blocks are composed of spherical-shaped nanoparticles connected to each other with individual sizes of around 10 nm. The Pr_6O_{11} nanoparticles possess a polycrystalline face-centred cubic phase.

5. References

[1] Shrestha S, Yeung C. M. Y., Nunnerley C., Tsang S. C (2007), Comparison of morphology and electrical conductivity of various thin films containing nano-crystalline praseodymium oxide particles, Sensors and Actuators A, 136: 191-198.

[2] Šulcová P (2005), Thermal synthesis of the CeO2-PrO2-Nd2O3 pigments, Journal of Thermal Analysis and Calorimetry, 82: 51-54.

[3] Asami K, Kusakabe K-I, Ashi N, Ohtsuka Y (1997), Synthesis of ethane and ethylene from methane and carbon dioxide over praseodymium oxide catalysts, Applied Catalysis A: General, 156: 43-56.

[4] Bernal S, Botana F. J, Cifredo G, Calvino J. J, Jobacho A, Rodriguez-Izquierdo J. M (1992), Preparation and characterization of a praseodymium oxide to be used as a catalytic support, Journal of Alloys and Compounds, 180: 271-279.

[5] Kawabe M, Ono H, Sano T, Tsuji M, Tamaura Y (1997), Thermochemical oxygen pump with praseodymium oxides using a temperature-swing at 403-873 K, Energy, 22: 1041-1049.

[6] Huang P. X, Wu F, Zhu B. L, Li G. R, Wang Y. L, Gao X. P, Zhu H. Y, Yan T. Y, Huang W. P, Zhang M, Song D. Y (2006), Praseodymium Hydroxide and Oxide Nanorods and Au/Pr6O11 Nanorod Catalysts for CO Oxidation, Journal of Physical Chemistry B, 110: 1614-1620.

[7] Ma L, Chen W, Zhao J, Zheng Y, Li X, Xu Z (2007), Microwave-assisted synthesis of praseodymium hydroxide nanorods and thermal conversion to oxide nanorod, Materials Letters, 61: 1711-1714.

[8] Matović B, Pantić J, Prekayski M, Stanković N, Bučevac D, Minović T, Čebela M (2013), Synthesis and characterization of Pr6O11 nanopowders, Ceramics International, 39: 3151-3155.

[9] Wang X, Zhuang J, Li Y. D (2004), Pr6O11 Single-Crystal Nanotubes from a Molten-Salt Synthetic Method, European Journal of Inorganic Chemistry, 5: 946-948.

[10] Yan L, Yu R, Liu G, Xing X (2008), A facile template-free synthesis of large-scale single crystalline Pr(OH)3 and Pr6O11 nanorods, Scripta Materialia, 58: 707-710.

[11] Hassan M. S, Kang Y. S, Kim B. S, Kim I.. S, Kim H. Y, Khill M. S (2011), Synthesis of praseodymium oxide nanofiber by electrospinning, Superlattices and microstructures, 50: 139-144.

[12] Borchert Y, Sonström P, Wihelm M, Borchert H, Bäumer M (2008), Nanostructured Praseodymium Oxide: Preparation, Structure, and Catalytic Properties, Journal of Physical Chemistry C, 112: 3054-3063.

[13] Salles V, Bernard S, Li J, Brioude A, Chehaidi S, Foucaud S , Miele P (2009), Design of Highly Dense Boron Nitride by the Combination of Spray-Pyrolysis of Borazine and Additive-Free Sintering of Derived Ultrafine Powders, Chemistry of Materials, 21: 2920-2929.

[14] Qi L (2010), Colloidal chemical approaches to inorganic micro- and nanostructures with controlled morphologies and patterns, Coordination Chemistry Reviews, 254: 1054-1071.

[15] Salles V, Bernard S, Brioude A, Cornu D, Miele P (2010), A new class of boron nitride fibers with tunable properties by combining an electrospinning process and the polymer-derived ceramics route, Nanoscale, 2: 215-217

[16] Gates B. D, Xu Q. B, Stewart M, Ryan D, Willson C. G, Whitesides G. M (2005) New Approaches to Nanofabrication: Molding, Printing, and Other Techniques, Chemical Reviews, 105: 1171-1196.

[17] Whitesides G. M, Grzybowski B (2002), Self-Assembly at All Scales, Science, 295: 2418-2421.

[18] Wild M, Berner S, Suzuki H, Rarnoino L, Baratoff A, Jung T. A, (2003), Molecular Assembly and Self-Assembly: Molecular Nanoscience for Future Technologies, Chimia, 56: 500-505.

[19] Zhang S (2003), Graphene: carbon in two dimensions, Review article, Materials Today, 6: 20-27.

[20] Rao C. N. R, Vivekchand S. R. C, Biswas K, Govindaraj A (2007), Synthesis of inorganic nanomaterials, Dalton Transactions, 6: 3728-3749.

[21] Wang Y, Zheng Y, Huang C. Z, Xia Y (2013), Synthesis of Ag Nanocubes 18-32 nm in Edge Length: The Effects of Polyol on Reduction Kinetics, Size Control, and Reproducibility, Journal of the American Chemical Society, 135: 1941-1951.

[22] Ikeda T, Xiong A, Yoshinaga T, Maeda K, Domen K, Teranishi T (2013), Polyol Synthesis of Size-Controlled Rh Nanoparticles and their Application to Photocatalytic Overall Water Splitting under Visible Light, Journal of Physical Chemistry C, 117: 2467-2473.

[23] Du H, Jiao L, Cao K, Wang Y, Yuan H (2013), Polyol-Mediated Synthesis of Mesoporous α-Ni(OH)2 with Enhanced Supercapacitance, ACS Applied Materials and Interfaces, 5: 6643-6648.

[24] Uchaker E, Zhou N, Li Y, Cao G (2013), Polyol-Mediated Solvothermal Synthesis and Electrochemical Performance of Nanostructured V2O5 Hollow Microspheres, Journal of Physical Chemistry C, 117: 1621-1626.

[25] Karipoth P, Thirumurugan A, Joscyphus R. J (2013), Synthesis and magnetic properties of flower-like FeCo particles through a one-pot polyol process, Journal of Colloid and Interface Science, 404: 49-55.

[26] Meetei S. D, Singh S. D, Sudarsan V (2012), Polyol synthesis and characterizations of cubic ZrO2:Eu3+ nanocrystals, Journal of Alloys Compounds, 514: 174-178.

[27] Shen L, Uchaker E, Yuan C, Nie P, Zhang M, Zhang X, Cao G (2012), Three-Dimensional Coherent Titania–Mesoporous Carbon Nanocomposite and its Lithium-Ion Storage Properties, ACS Applied Materials and Interfaces, 4: 2985-2992.

[28] Shen L, Zhang X, Uchaker E, Yuan C, Cao G (2012), Li4Ti5O12 Nanoparticles Embedded in a Mesoporous Carbon Matrix as a Superior Anode Material for High Rate Lithium Ion Batteries, Advanced Energy Materials, 2: 691-698.

[29] Feldmann, Merikhi C and J (2003), Synthesis and characterization of rod-like Y2O3 and Y2O3:Eu3+, Journal of Materials Science, 38: 1731-1735.

[30] Lee S, Jeong S, Kim D, Hwang S, Jeon M, Moon J (2008), ZnO nanoparticles with controlled shapes and sizes prepared using a simple polyol synthesis, Superlattices and Microstructures, 43: 330-339.

[31] Sicard L, Le Meins J. M, Méthivier C, Herbst F, Ammar S (2010), Polyol synthesis and magnetic study of Mn3O4 nanocrystals of tunable size, Journal of Magnetism and Magnetic Materials, 322: 2634-2640.

[32] Siemons M, Simon U (2007), Gas sensing properties of volume-doped CoTiO3 synthesized via polyol method, Sensors and Actuators B: Chemical, 126: 595-603.

[33] Ragupathy P, Shivakumara S, Vasan H. N, Munichandraiah N (2008), Preparation of Nanostrip V2O5 by the Polyol Method and its Electrochemical Characterization as Cathode Material for Rechargeable Lithium Batteries, Journal of Physical Chemistry C, 112: 16700-16707.

[34] Jiang X. C, Herricks T, Xia Y. N (2003), Monodispersed Spherical Colloids of Titania: Synthesis, Characterization, and Crystallization, Advanced Materials, 15: 1205-1209.

[35] Jiang X. C, Wang Y. L, Herricks T, Xia Y. N (2004), Ethylene glycol-mediated synthesis of metal oxide nanowires, Journal of Materials Chemistry, 14: 695-703.

[36] Flores-Gonzalez M. A, Ledoux G, Roux S, Lebboua K, Perriat P, Tillement O (2005), Preparing nanometer scaled Tb-doped Y2O3 luminescent powders by the polyol method, Journal of Solid State Chemistry, 178: 989-997.

[37] Zhou N, Liu Y, Li J, Uchaker E, Liu S, Huang K, Cao G (2012), Synthesis and characterization of high power LiFePO4/C nano-plate thin films, Journal of Power Sources, 213: 100-105.

[38] Sun Y. G, Yin Y. D, Mayers B. T, Herricks T, Xia Y. N (2002), Uniform silver nanowires synthesis by reducing $AgNO_3$ with ethylene glycol in the presence of seeds and poly(vinyl pyrrolidone), Chemistry of Materials, 14: 4736-4745.

[39] Feldmann C (2003), Polyol-Mediated Synthesis of Nanoscale Functional Materials, Advanced Functional Materials, 13: 101-107.

[40] Majoulet O, Bechelany M. C, Sandra F, Bonnefont G, Fantozzi G, Joly-Pottuz L, Malchere A, Bernard S, Miele P (2013), Silicon-boron-carbon-nitrogen monoliths with high, interconnected and hierarchical porosity, Journal of Materials Chemistry A, 1: 10991-11000.

[41] Bernard S, Miele P (2013), Polymer-Derived Ordered Mesoporous Silicon-Boron-Carbon-Nitrogen (Si/B/C/N) Ceramics, Journal of Ceramic Science Technology, 4: 113-122.

[42] Bernard S, Majoulet O, Sandra F, Malchere A, Miele P (2013), Direct synthesis of periodic mesoporous SilicoBoron CarboNitride frameworks via the nanocasting from ordered mesoporous silica with boron-modified polycarbosilazane, Advanced Engineering Materials, 15: 134-140.

[43] Schlienger S, Alauzun J, Michaux F, Vidal L, Parmentier J, Gervais C, Babonneau F, Bernard S, Miele P, Parra J. B (2012), Micro-, Mesoporous boron nitride-based materials templated from zeolites, Chemical Materials, 24: 88-96.

[44] Alauzun J. G, Ungureanu S, Brun N, Bernard S, Miele P, Backov R, Sanchez C (2011), Novel monolith-type boron nitride hierarchical foams obtained through integrative chemistry, Journal of Materials Chemistry, 21: 14025-14030.

[45] Majoulet O, Alauzun J. G, Gottardo L, Gervais, Schuster M. E, Bernard S, Miele P (2011), Ordered mesoporous silicoboron carbonitride ceramics from boron-modified polysilazanes: Polymer synthesis, processing and properties, Microporous and Mesoporous Materials, 140: 40-50.

[46]Yan X.-.B, Dibandjo P, Bernard S, Gottardo L, Mouttaabidd H, Miele P (2008), Ordered Mesoporous Silicoboron Carbonitride Materials via Preceramic Polymer Nanocasting, Chemistry of Materials, 20: 6325-6334.

[47] Kim M, Hinklin T. R, Laine R. L (2008), B Cation Ordered Double Perovskite Ba2CoMo0.5Nb0.5O6-delta as a Potential SOFC Cathode, Chemistry of Materials, 20: 5154-5162

[48] Hinklin T, Toury B, Gervais C, Babonneau F, Gislason J. J, Morton R. W, Laine R. M (2004), Liquid-Feed Flame Spray Pyrolysis of Metalloorganic and Inorganic Alumina Sources in the Production of Nanoalumina Powders, Chemistry of Materials, 16: 21-30.

[49] Azurdia J. A, Marchal J, Shea P, Sun H, Pan X. Q, Laine R. M (2006), Liquid-Feed Flame Spray Pyrolysis as a Method of Producing Mixed-Metal Oxide Nanopowders of Potential Interest as Catalytic Materials. Nanopowders along the NiO−Al2O3 Tie Line Including (NiO) 0.22(Al2O3)0.78, a New Inverse Spinel Composition, Chemistry of Matererials, 18: 731-739.

[50] International Union of Pure and Applied Chemistry (1985), Reporting physisorption data for gas/solid systems, Pure and Applied Chemistry, 57: 603-619

[51] International Union of Pure and Applied Chemistry (1994), Recommendation for the characterisation of porous solids, Pure and Applied Chemistry, 66: 1739-1758.